Journal of Computational Physics 228 (2009) 8908–8918

Contents lists available at ScienceDirect

Journal of Computational Physics

journal homepage: www.elsevier.com/locate/jcp

A family of functions for mass and energy flux splitting of the Euler equations

A.C. Raga [a,*], J. Cantó [b]

[a] Instituto de Ciencias Nucleares, UNAM, Ap. 70-543, 04510 DF, Mexico
[b] Instituto de Astronomía, UNAM, Ap. 70-264, 04510 DF, Mexico

ARTICLE INFO

Article history:
Received 9 December 2008
Received in revised form 31 August 2009
Accepted 3 September 2009
Available online 11 September 2009

Keywords:
Flux vector splitting schemes
Shock capturing technique

ABSTRACT

Flux vector splitting algorithms for the Euler equations are based on dividing the mass, momentum and energy fluxes into a "forward directed flux" F^+ and a "backward directed flux" F^- (with $F^- = 0$ for Mach numbers $M > 1$ and $F^+ = 0$ for $M < -1$). van Leer (1979, 1982) [4,5] proposed using polynomials of the Mach number for computing F^+ and F^- in the subsonic regime, and derived the lowest order polynomials that satisfy a set of chosen criteria. In this paper, we explore the possibility of increasing the order of these polynomials, with the purpose of reducing the diffusion across slow moving contact discontinuities of the flux vector splitting algorithm. We find that a moderate reduction of the diffusion, resulting in sharper shocks and contact discontinuities, can indeed be obtained with the higher order polynomials for the split fluxes.

1. Introduction

Steger and Warming [1] proposed an algorithm based on splitting the mass, momentum and energy fluxes of the Euler equations into a "forward" and a "backward" flux, having positive and negative eigenvalues (respectively) of their associated Jacobian matrices. van Leer [4,5] proposed an alternative form for the split fluxes in the subsonic regime, as polynomials of the Mach number. Recent developments in flux vector splitting algorithms include the work of Sun and Takayama [2] and Sengupta et al. [3].

The flux vector splitting algorithm of van Leer [4,5] has been extensively used in astrophysical applications (e.g. [9,10]), mostly in implementations with second order spatial and temporal accuracy. At the heart of the algorithms which are used are the polynomials calculated by van Leer for interpolating the split fluxes in the subsonic regime.

In the present paper, we calculate a set of polynomials of increasing orders of the Mach number for the mass and energy split fluxes. These polynomials are designed to minimize the mass and energy diffusion through structures such as slow moving contact discontinuities. We then illustrate the behaviour of the proposed fluxes with an application to one of the one-dimensional tests proposed by Toro [7].

We should note that Coirier and van Leer [6] presented Mach number polynomials designed with the same objective of lowering the diffusion at low Mach numbers. Their polynomials, however, led to at best marginally stable numerical solutions.

The paper is organized as follows. In Section 2, we write the Euler equations in the appropriate form for the derivation of the Mach number polynomials. In Section 3, we describe the split fluxes of van Leer [4,5] and of Coirier and van Leer [6]. In Section 4, we derive our new mass and energy split fluxes. In Section 5, we present an analysis of the eigenvalues of these

* Corresponding author. Tel.: +52 55 56 22 46 72; fax: +52 55 56 16 22 33.
E-mail address: raga@nucleares.unam.mx (A.C. Raga).

0021-9991/$ - see front matter © 2009 Elsevier Inc. All rights reserved.
doi:10.1016/j.jcp.2009.09.006

fluxes. In Section 6 we discuss a numerical test with a first order implementation of the FVS scheme, and in Section 7 we analyse the linear stability of this scheme. Finally, in Section 8 we present a summary of the results.

2. The Euler equations

We write the 1D Euler equations in conservative form:

$$\frac{\partial U}{\partial t}+\frac{\partial F}{\partial x}=0, \tag{1}$$

where

$$U(M,\rho,c_s)=\begin{pmatrix}\rho\\ \rho c_s M\\ \rho c_s^2[M^2/2+1/\gamma(\gamma-1)]\end{pmatrix}, \tag{2}$$

$$F(M,\rho,c_s)=\begin{pmatrix}F_m\\ F_p\\ F_e\end{pmatrix}=\begin{pmatrix}\rho c_s M\\ \rho c_s^2(M^2+1/\gamma)\\ \rho c_s^3 M[M^2/2+1/(\gamma-1)]\end{pmatrix}, \tag{3}$$

are the integrated variables (U) and fluxes (F) written in terms of the flow density ρ, the sound speed $c_s=\sqrt{\gamma P/\rho}$ (where γ is the specific heat ratio) and the Mach number M.

3. van Leer's fluxes

In a flux vector splitting algorithm, the mass, momentum and energy fluxes are divided into a "forward directed flux" F^+ (i.e., moving in the $+x$-direction) and a "backward directed flux" F^-. For the supersonic regime, the F^+ and F^- fluxes are chosen as

$$F^+=F,\quad F^-=0\quad \text{for } M>1;\quad F^-=F,\quad F^+=0\quad \text{for } M<-1. \tag{4}$$

The conditions that van Leer [4,5] imposes in order to derive his split fluxes in the $-1\leqslant M\leqslant 1$ regime are:

1. $F=F^++F^-$,
2. dF^+/dU must have all eigenvalues $\geqslant 0$ and dF^-/dU must have all eigenvalues $\leqslant 0$,
3. F^+ and F^- must be continuous, with $F^+=F$ for $M\geqslant 1$ and with $F^-=F$ for $M\leqslant -1$,
4. the components of F^+ and F^- must mimic the symmetry of F with respect to M. In other words $F^+(M)=\pm F^-(-M)$ if $F(M)=\pm F(-M)$,
5. $dF^\pm/dU$ must be continuous,
6. $dF^\pm/dU$ must have one eigenvalue vanish for $|M|<1$,
7. $F^\pm(M)$ must be a polynomial in M, of the lowest possible order.

With these conditions, van Leer [5] derives the polynomials:

$$F_m^+=\rho c_s\frac{(M+1)^2}{4}, \tag{5}$$

$$F_p^+=\rho c_s^2\frac{(M+1)^2}{4\gamma}[(\gamma-1)M+2], \tag{6}$$

$$F_e^+=\rho c_s^3\frac{(M+1)^2}{8(\gamma^2-1)}[(\gamma-1)M+2]^2, \tag{7}$$

for the three components of the flux vector (see Eq. (3)).

Actually, the polynomials are derived without imposing a priori condition 2 (see above). van Leer [5] a posteriori checks that the fluxes given by Eqs. (5)–(7) do satisfy condition 2.

A weakness of flux vector splitting algorithms is the fact that they produce relatively large mass and energy diffusion across slow moving contact discontinuities. This diffusion is associated with the fact that even though $F_m^++F_m^-=F_m=\rho cM$ (see condition 1 above and Eq. (3)) go to zero for $M\to 0$, the moduli of the individual forward and backward mass fluxes have large values $|F_m^\pm(M=0)|=\rho c_s/4$ (see Eq. (5)). A similar situation is found for the energy fluxes, which have $|F_e^\pm(M=0)|=\rho c_s^3/2(\gamma^2-1)$ (see Eq. (7)).

Coirier and van Leer [6] derived polynomials for $F_{m,e}^+$ with lower values at low Mach numbers. Their polynomials have negative $F_{m,e}^+$ for part of the $-1<M<0$ range (in other words, they have a negative "forward directed" flux). We have experimented with recipes giving negative $F_{m,e}^+$ (for a limited Mach number range), and find that in many conditions they produce

a strong anti-diffusion, which results in unstable numerical integrations. These results are consistent with the conclusions obtained by Coirier and van Leer [6].

In the following section, we derive polynomials for the forward and backward mass and energy fluxes which satisfy the condition $F^+_{m,e} > 0$ (in principle implicit in the general idea of having a flux vector splitting method) but have lower absolute values at low Mach numbers. Such fluxes should produce lower diffusion across slow moving contact discontinuities.

4. The mass and energy fluxes

We derive the mass and energy flux splitting by replacing conditions 6 and 7 of van Leer [5] with the conditions:

6. $F^\pm$ must have no zeros, local maxima or minima for $-1 \leqslant M \leqslant 1$,
7. $F^\pm(M)$ must be the polynomials in M of order p that satisfy the above conditions and have the lowest possible value of $|F^\pm(0)|$.

With conditions 1 and 3–5 of Section 3 and conditions 6–7 (see above), we derive polynomials of different orders p for the forward oriented mass and energy fluxes (F^+_m and F^+_e, respectively, see Eq. (3)). Condition 4 (see Section 3) eliminates odd values of p. Also, $p = 2$ is the lowest possible order for F^+_m and $p = 4$ is the lowest possible order for the polynomial for F^+_e.

The resulting polynomials with $p \leqslant 10$ then are:

2nd order ($p = 2$):

$$\frac{F^+_m}{\rho c_s} = \frac{(M+1)^2}{4}, \tag{8}$$

4th order ($p = 4$):

$$\frac{F^+_m}{\rho c_s} = \frac{(M+1)^3}{16}(3-M), \tag{9}$$

$$\frac{F^+_e}{\rho c_s^3} = \frac{(M+1)^3}{32(\gamma-1)}[7-\gamma-(5-3\gamma)M], \tag{10}$$

6th order ($p = 6$):

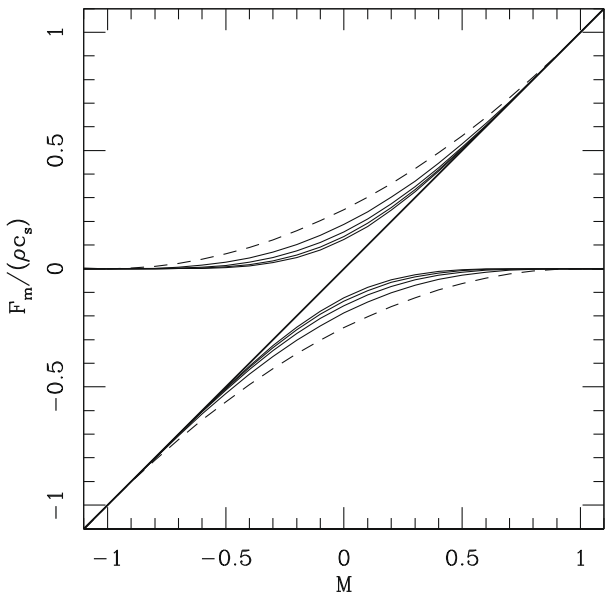

Fig. 1. Split mass fluxes F^+_m and F^-_m (normalized to ρc_s) obtained for the polynomials of order $p = 2$, 4, 6, 8 and 10 (Eqs. (8), (9), (11), (13) and (15)) as a function of the Mach number M. The positive curves correspond to F^+_m and the negative curves to F^-_m. The dashed curves correspond to the $p = 2$ polynomial (which is identical to van Leer's split mass flux), and the curves with successively lower absolute values correspond to the $p = 4$, 6, 8 and 10 solutions. The straight line that bisects the graph corresponds to the $F_m = \rho c_s M$ mass flux of the Euler equations.

$$\frac{F_m^+}{\rho c_s} = \frac{(M+1)^4}{32}(M^2 - 4M + 5), \tag{11}$$

$$\frac{F_e^+}{\rho c_s^3} = \frac{(M+1)^4}{64(\gamma-1)}[11 - \gamma - 4(3-\gamma)M + (3-\gamma)M^2], \tag{12}$$

8th order ($p = 8$):

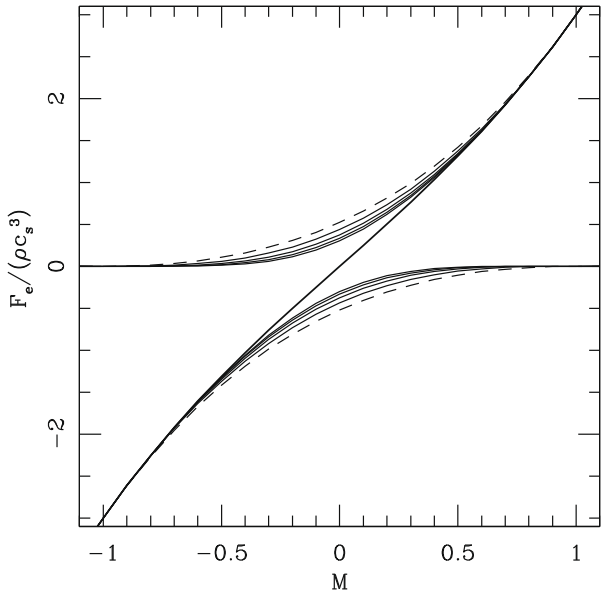

Fig. 2. Split energy fluxes F_e^+ and F_e^- (normalized to ρc_s^3) obtained from van Leer's polynomial (dashed line, Eq. (7)) and from our polynomials of order $p = 4$, 6, 8 and 10 (Eqs. (10), (12), (14) and (16)) as a function of the Mach number M. The positive curves correspond to F_e^+ and the negative curves to F_e^-. The solid curves with successively lower absolute values correspond to the $p = 4$, 6, 8 and 10 solutions. The curve that bysects the graph corresponds to the energy flux of the Euler equations (see Eq. (3)).

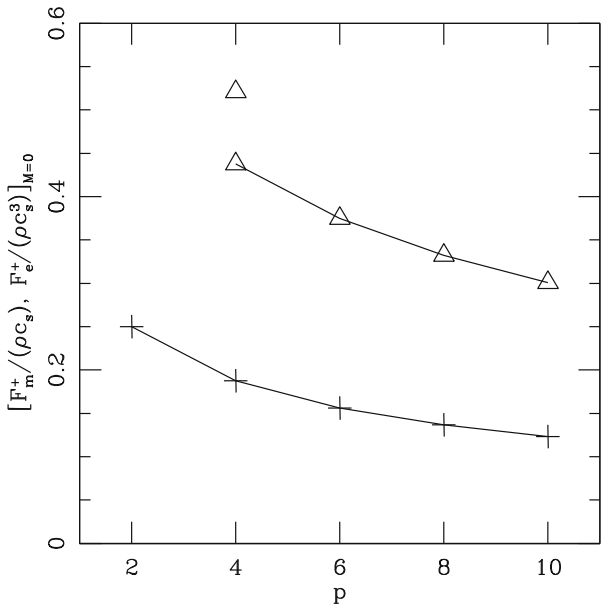

Fig. 3. Values of the forward mass flux (F_m^+, normalized to ρc_s: crosses) and the forward energy flux (F_e^+, normalized to ρc_s^3: triangles) at $M = 0$ as a function of the order p of the polynomials. The values obtained with our polynomials (Eqs. (8)–(16)) are joined with the solid curves. The isolated triangle corresponds to van Leer's energy flux (Eq. (7)).

$$\frac{F_m^+}{\rho c_s} = \frac{5(M+1)^5}{256}\left(7 - \frac{47}{5}M + 5M^2 - M^3\right), \tag{13}$$

$$\frac{F_e^+}{\rho c_s^3} = \frac{(M+1)^5}{512(\gamma-1)}[5(15-\gamma) - (119-25\gamma)M + 5(13-3\gamma)M^2 - (13-3\gamma)M^3], \tag{14}$$

10th order ($p = 10$):

$$\frac{F_m^+}{\rho c_s} = \frac{7(M+1)^6}{512}\left(M^4 - 6M^3 + \frac{102}{7}M^2 - \frac{122}{7}M + 9\right), \tag{15}$$

$$\frac{F_e^+}{\rho c_s^3} = \frac{(M+1)^6}{1024(\gamma-1)}[7(19-\gamma) - 2(143-21\gamma)M + 6(41-7\gamma)M^2 - 6(17-3\gamma)M^3 + (17-3\gamma)M^4]. \tag{16}$$

Figs. 1 and 2 show the functions given by Eqs. (8)–(16) for $\gamma = 1.4$. The second order mass flux polynomial coincides with the mass flux of van Leer (Eq. (5)). Our fourth order energy flux (Eq. (10)), however, does not coincide with the corresponding fourth order polynomial of van Leer (see Eq. (7)), having a lower $F_e^+(M=0)$ value (see Fig. 2).

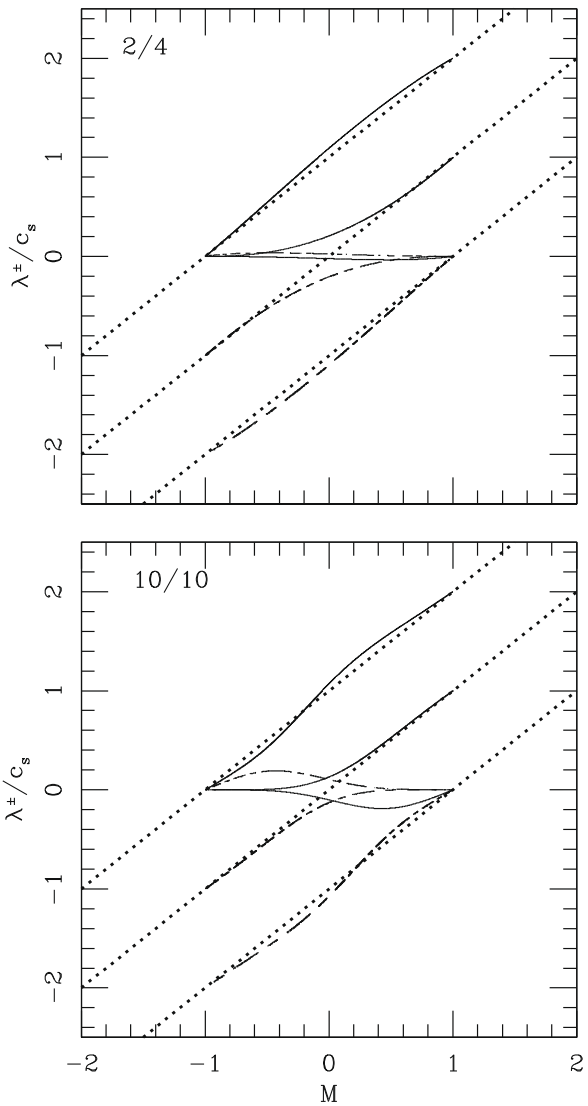

Fig. 4. Eigenvalues λ^+ of F^+ (solid lines) and λ^- of F^- (dashed lines) as a function of Mach number M. The dotted lines correspond to the eigenvalues $\lambda_1 = (M-1)c_s$, $\lambda_2 = Mc_s$ and $\lambda_3 = (M+1)c_s$ of the Euler equations. The top plot shows the eigenvalues obtained for the combination of our $p = 2$ mass flux polynomial (Eq. (8)) and our $p = 4$ energy flux (Eq. (10)). The bottom plot corresponds to the combination of our $p = 10$ mass and energy fluxes (Eqs. (15) and (16)). In both cases, van Leer's momentum flux was used (Eq. (6)).

As we have described in Section 3, the mass and energy diffusion for contact discontinuities at rest is associated with the non-zero values of $F^+_{m,e}$ for $M = 0$, i.e., with the values of $F^-_{m,e}(M = 0) = -F^+_{m,e}(M = 0)$. In Fig. 3, we plot the values of $F^+_{m,e}(M = 0)$ for the polynomials of Eqs. (8)–(16), and also for van Leer's energy flux (Eq. (7)). From this figure, we see that our $p = 10$ polynomials have fluxes at $M = 0$ with values of $\approx 1/2$ of the corresponding values of van Leer's fluxes.

5. The eigenvalues of $dF^{\pm}/dU$

The remaining point in the derivation of the new polynomials for F^+ (Eqs. (8)–(16)) and F^- (calculated through the condition $F^- = F - F^+$, with F given by Eq. (3)) satisfy van Leer's condition number 2 (see Section 3), namely, that the Jacobian matrix dF^+/dU must have all eigenvalues $\lambda^+ \geqslant 0$ and that dF^-/dU must have all eigenvalues $\lambda^- \leqslant 0$. These two relations are satisfied by the fluxes given by van Leer's polynomials (Eqs. (5)–(7)).

In Fig. 4, we show the eigenvalues $\lambda^{\pm}$ (corresponding to the $F^{\pm}$ fluxes) obtained for a $\gamma = 1.4$ specific heat ratio for two combinations:

- 2/4: the $p = 2$ mass flux polynomial (Eq. (8)) and the $p = 4$ energy flux polynomial (Eq. (10)).
- 10/10: the $p = 10$ mass and energy flux polynomials (Eqs. (15) and (16)).

In both cases, van Leer's momentum flux (Eq. (6)) has been included.

From Fig. 4, we see that for the 2/4 case we obtain two eigenvalues λ^+ for F^+ that monotonically grow from 0 at $M = -1$ to values of c_s and $2c_s$ at $M = 1$. The third eigenvalue is negative, but has a modulus ~ 2 orders of magnitude smaller than the other two eigenvalues (analogously, F^- has one eigenvalue which is small but positive). Therefore, the conditions of positive eigenvalues for F^+ and negative eigenvalues for F^- is not strictly met, though the values of the λ's with the "wrong signs" are small.

For the 10/10 case we obtain a similar behaviour for the eigenvalues (see Fig. 4), with the qualitative difference that the negative λ^+ has moduli of $\sim 1/10$ of the values of the positive eigenvalues. Therefore, the condition of $\lambda^+ > 0$ is violated more strongly than in the $p = 2/4$ case.

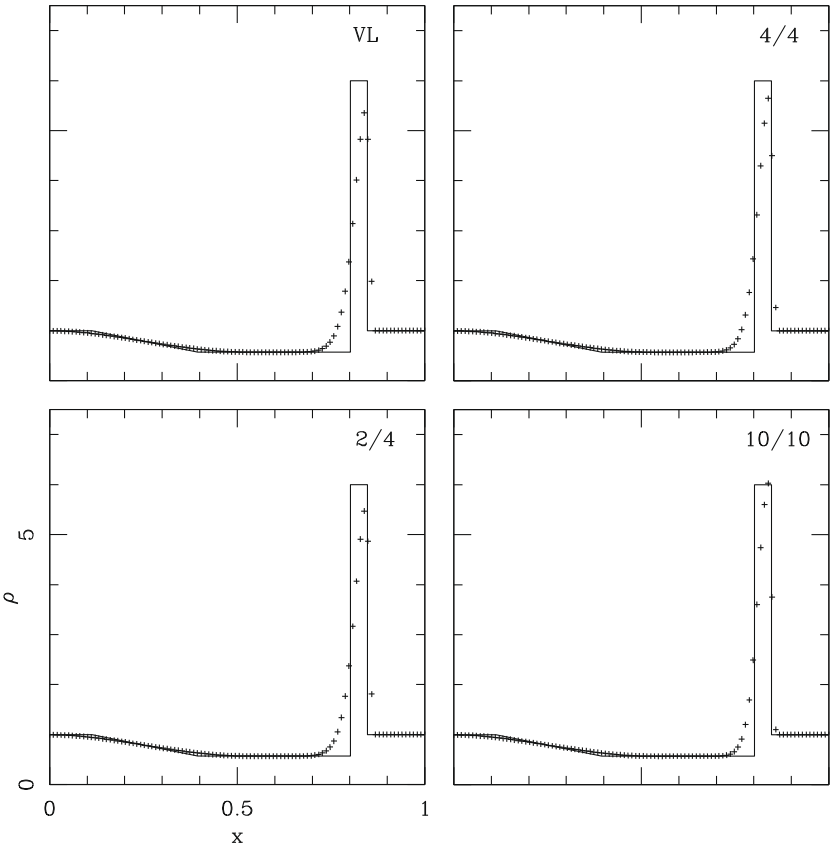

Fig. 5. Density structure obtained for the 1D test problem described in Section 6. Counterclockwise from top left, we have the results obtained with: van Leer's fluxes, the $p = 2$ mass flux/$p = 4$ energy flux combination, the $p = 4$ mass flux/$p = 4$ energy flux combination, and the $p = 10$ mass flux/$p = 10$ energy flux combination.

An interesting property of the eigenvalues of the F^+ fluxes given by the 10/10 combination is that they join the $\lambda = v + c$, v and $v - c$ eigenvalues of the Euler fluxes (Eq. (3)) with continuous derivatives at $M = 1$. The same thing is evidently found for the λ^- values at $M = -1$ (see Fig. 4). The price one pays for this smoother joining between the subsonic and supersonic $F^\pm$ fluxes is to have one negative λ^+ (and positive λ^-) in the $|M| < 1$ regime.

6. Numerical test

In order to illustrate the behaviour of the fluxes derived in Section 4, we show results obtained with a first order implementation of the flux vector splitting algorithm. We use a timestepping procedure of the form:

$$U_j(t + \Delta t) = U_j(t) + \left(\frac{\Delta t}{\Delta x}\right)\left[F^+_j(t) + F^-_{j+1}(t) - F^-_j(t) - F^+_{j-1}(t)\right]. \tag{17}$$

We present the results obtained for one of the tests suggested in the book of Toro [7]. We start with a domain with a spatial extent $L = 1$, which is resolved with 100 grid points. The initial condition is a step function with $\rho_l = 1,\ P_l = 1000,\ v_l = -19.59745$ on the left, and $\rho_r = 1,\ P_r = 0.01,\ v_r = -19.59745$ on the right. The discontinuity is located at a position $x_0 = 0.8$, and the specific heat ratio has a value $\gamma = 1.4$.

Starting with this initial condition, the integration is advanced with a Courant number of 0.6 (except for the five first steps, which are advanced with a Courant number of 0.12), for a total time $t_m = 0.12$. The last timestep is reduced so as not to exceed t_m. This is the setup used by Toro [7], so that the results obtained in his book for this test with different algorithms are directly comparable to the results that we present here.

In Figs. 5–8, we show the flow obtained at the time $t_m = 0.12$ for different choices of the mass and energy fluxes. We have chosen the following flux combinations:

- VL: van Leer's fluxes (Eqs. (5)–(7)),
- 2/4: the $p = 2$ mass flux and $p = 4$ energy flux (Eqs. (8) and (10)),
- 4/4: the $p = 4$ mass flux and $p = 4$ energy flux (Eqs. (9) and (10)),
- 10/10: the $p = 10$ mass flux and $p = 10$ energy flux (Eqs. (15) and (16)).

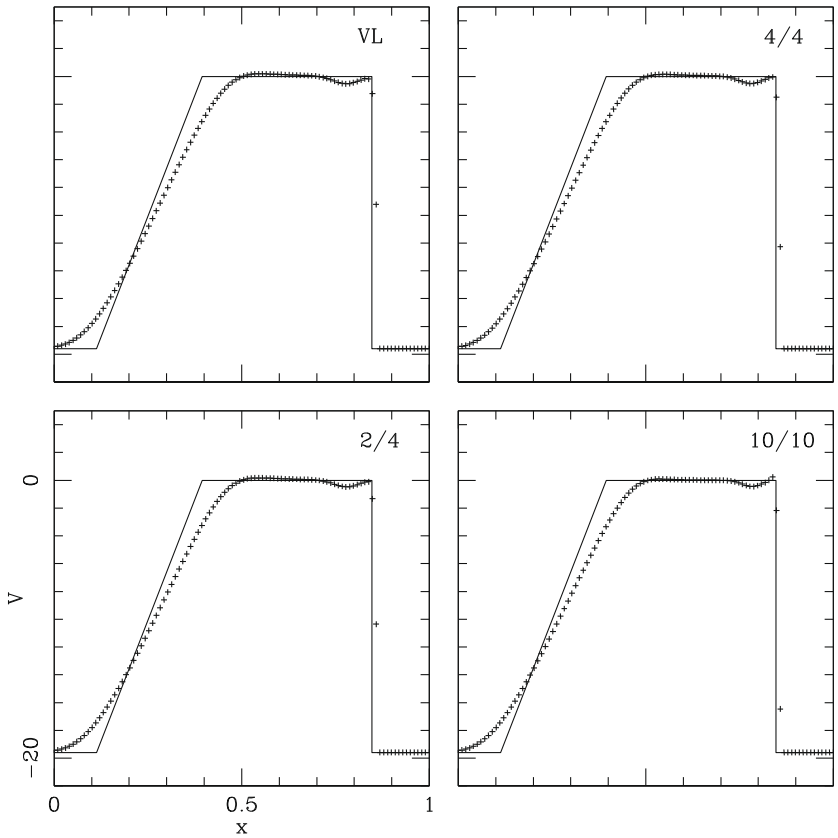

Fig. 6. Velocity structure obtained for the 1D test problem described in Section 6 (also see Fig. 1).

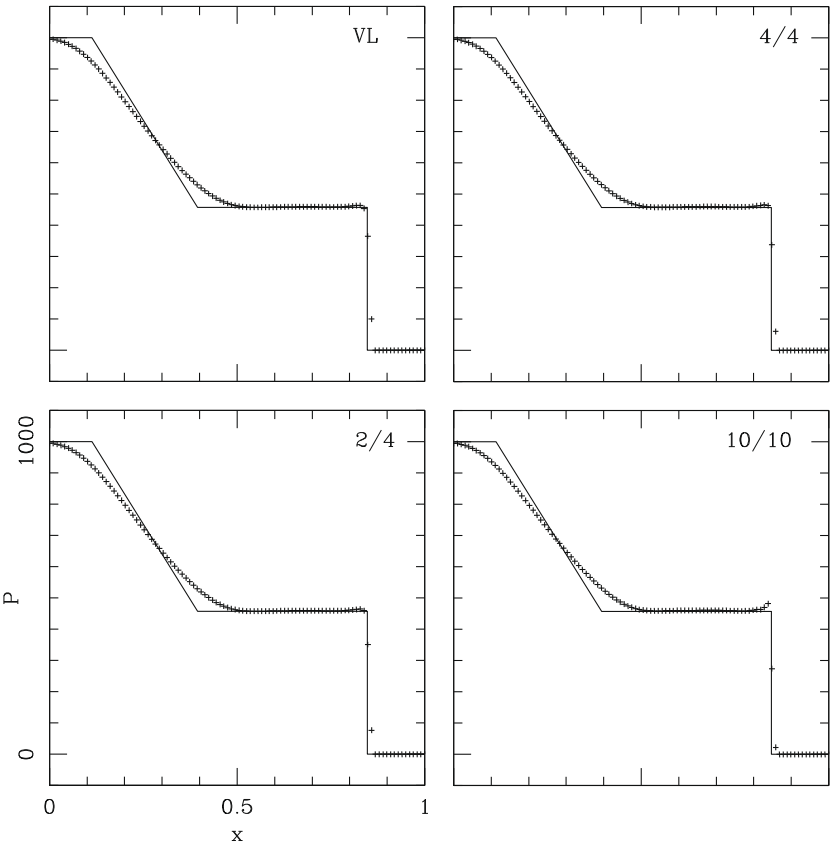

Fig. 7. Pressure structure obtained for the 1D test problem described in Section 6 (also see Fig. 1).

In all cases the momentum flux is the one of van Leer (Eq. (6)).

In the density stratifications shown in Fig. 5, we find lower diffusion as one progresses from VL to 2/4, 4/4 and 10/10. This is seen as a narrowing of the contact discontinuity, and as an increase in the values of the densities in the region between the contact discontinuity and the shock. For the 10/10 fluxes, the correct density (corresponding to the factor of 6 compression in the strong, $\gamma = 1.4$ shock) is obtained in one pixel within this region.

For the VL solution, we find that the maximum density jump between two successive cells within the contact discontinuity is $(\Delta\rho)_{\rm VL} = 0.86$. For the 10/10 solution, the maximum density jump within the contact discontinuity is $(\Delta\rho)_{10/10} = 1.10$. Therefore, the contact discontinuity in the 10/10 solution is a factor of $(\Delta\rho)_{\rm VL}/(\Delta\rho)_{10/10} = 0.78$ narrower than in the VL solution.

Fig. 6 shows the flow velocity v obtained at the time $t_m = 0.12$ (see above). Very similar results are obtained for the four choices of the fluxes. The maximum velocity jump between two successive pixels within the shock grows from $(\Delta v)_{\rm VL} = 10.4$ with van Leer's fluxes to $(\Delta v)_{10/10} = 14.3$ with the tenth order fluxes. Therefore, the shock in the 10/10 solution is a factor of $(\Delta v)_{\rm VL}/(\Delta v)_{10/10} = 0.73$ narrower than in the VL solution.

Fig. 7 shows the pressure stratifications. These are very similar for all flux combinations, and show a narrowing of the shock transition which is similar to the one seen in the density stratifications (see above and Fig. 5). An overshoot in the postshock pressure develops as one goes to the higher order flux solutions. This overshoot is clearly seen in the 10/10 solution (see Fig. 7).

Finally, in Fig. 8 we show the stratifications of the thermal energy per unit mass $E_T = P/(\gamma - 1)\rho$. As one goes to higher order fluxes, an improvement is obtained in the definition of the "step" in between the shock and the contact discontinuity. The maximum thermal energy jump between two successive pixels within the contact discontinuity grows from $(\Delta E_T)_{\rm VL} = 220$ with van Leer's fluxes to $(\Delta E_T)_{10/10} = 303$ with the tenth order fluxes. Therefore, the contact discontinuity in the 10/10 solution is a factor of $(\Delta E_T)_{\rm VL}/(\Delta E_T)_{10/10} = 0.73$ narrower than in the VL solution.

7. Linear stability

As a final point, we analyse the stability of the first order time-stepping algorithm we have used in Section 6 (Eq. (17)). We assume that the error ξ satisfies a linear advection equation:

$$\frac{\partial \xi}{\partial t} + v\frac{\partial \xi}{\partial x} = 0, \tag{18}$$

where $v = u + c_s$ is the maximum wave propagation speed in a constant velocity flow with $u > 0$.

Applying the time-stepping algorithm of Eq. (17), we have

$$\xi_j(t+\Delta t) = \xi_j(t) - Co\left[\xi_j^+(t) + \xi_{j+1}^-(t) - \xi_j^-(t) - \xi_{j-1}^+(t)\right], \tag{19}$$

where $Co = v\Delta t/\Delta x$ is the Courant number. Through the flux vector splitting algorithm, we can determine the ratio $f = \xi_j^+/\xi_j$. Introducing $\xi_j^+ = f\xi_j$ and $\xi_j^- = (1-f)\xi_j$ in Eq. (19), we obtain

$$\xi_j(t+\Delta t) = \xi_j(t) - Co[(2f-1)\xi_j(t) + (1-f)\xi_{j+1}(t) - f\xi_{j-1}(t)]. \tag{20}$$

For $f = 1$ this equation is an upwind differencing scheme, and for $f = 1/2$ it corresponds to a CDFT (centred difference, forward time) scheme, known to be unstable. For $f \gg 1$, Eq. (20) takes the form

$$\xi_j(t+\Delta t) \approx \xi_j(t) + fCo[\xi_{j+1}(t) + \xi_{j-1}(t) - 2\xi_j(t)], \tag{21}$$

namely, the second-order finite difference operator for a diffusion equation with diffusion coefficient $D = fCo(\Delta x)^2/\Delta t$.

We now substitute a Fourier component e^{nt+ikx} (with $k = 0 \to \pi/\Delta x$) of the error ξ into Eq. (20), and compute the value of the Courant number Co_s for marginal stability (i.e., for $|e^{nt}| = 1$), obtaining

$$Co_s = \frac{(2f-1)(1-\cos k\Delta x)}{(2f-1)^2(1-\cos k\Delta x)^2 + 1 - \cos^2 k\Delta x}. \tag{22}$$

In Fig. 9 we show the values obtained from this equation for Co_s as a function of $f = \xi^+/\xi$ and $\cos k\Delta x$. In this figure, we see that for $f = 0.5$ (corresponding to the lowest value of f shown in the ordinate) we have $Co_s = 0$ (as appropriate for the unstable FTCD scheme, see above), and for $f = 1$ we have $Co_s = 1$ (appropriate for an upwind differencing scheme, see above). Values $f < 1/2$ result in negative values for Co_s (see Eq. (22)), so they are not shown in Fig. 9.

FVS schemes with positive F^+ and negative F^- (imposed by condition 6′ of Section 4 when applied to the mass and momentum fluxes) have $f > 1$. In this region of the plot shown in Fig. 9, we see that Co_s is a monotonically growing function

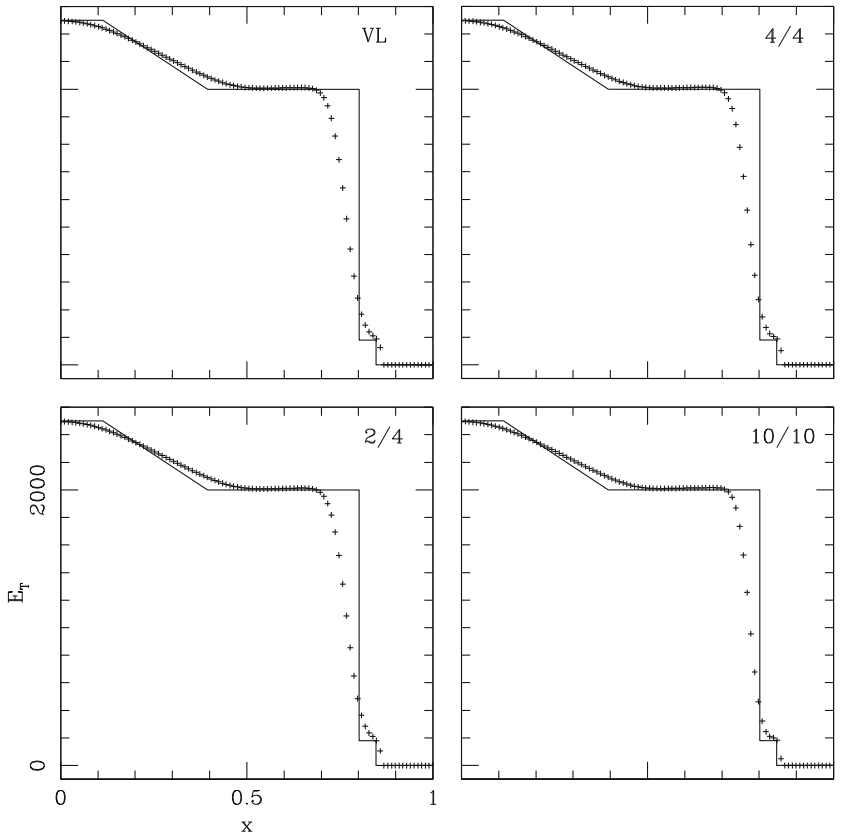

Fig. 8. Thermal energy ($E_T = P/(\gamma-1)\rho$) structure obtained for the 1D test problem described in Section 6 (also see Fig. 1).

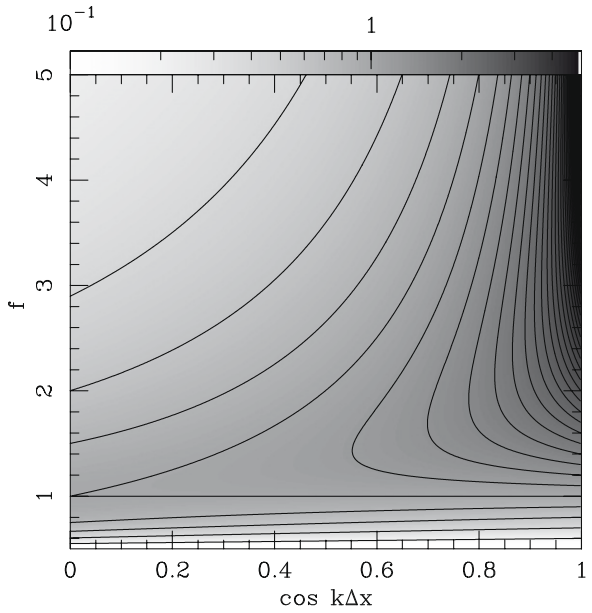

Fig. 9. Courant number Co_s for marginal stability of the first order FVS algorithm, as a function of $\cos k\Delta x$ and $f = \xi^+/\xi$ (see Eq. (22)). The values of Co_s are represented with a logarithmic greyscale and with contours corresponding to a linear spacing of 0.1 (with the straight, horizontal contour at $f = 1$ corresponding to $Co_s = 1$).

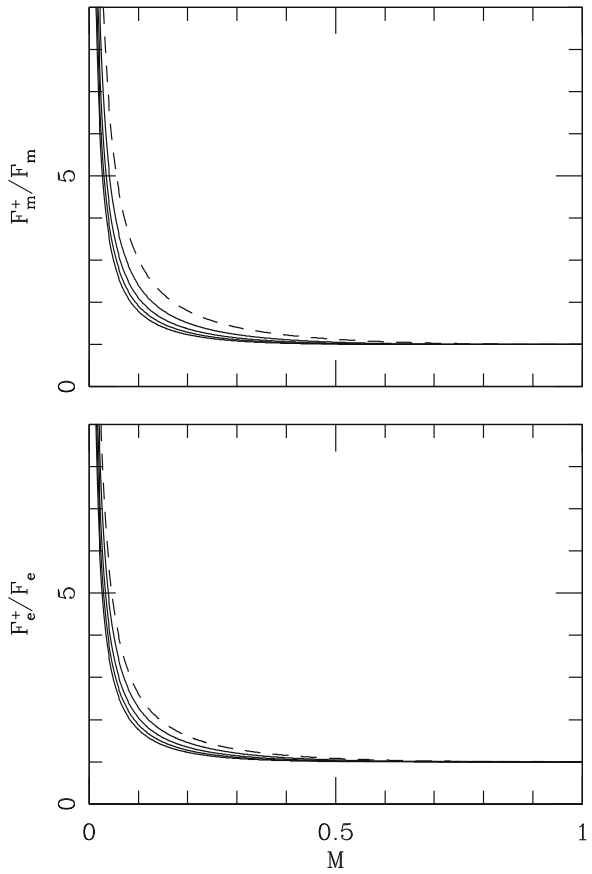

Fig. 10. Values of F_m^+/F_m (top) and F_e^+/F_e (bottom) as a function of Mach number M. The values obtained with van Leer's polynomials (see Section 3) are shown with the dashed lines. The values obtained with our higher order polynomials (see Section 4) are shown with the solid lines, except for the case of our lowest order F_m^+, which is identical to van Leer's forward mass flux. The curves corresponding to higher order polynomials have lower values of F^+/F for all values $M < 1$.

of $\cos k\Delta x$. Therefore, the time step will be limited by the requirement of stability for the shortest wavelength mode (with $\cos k\Delta x = 0$) of the error. For this mode, Eq. (22) gives

$$Co_s = \frac{2f-1}{(2f-1)^2+1}, \tag{23}$$

so that $Co_s = 1/(2f)$ for $f \gg 1$. Therefore, for large values of f, the maximum stable timestep ($\Delta t_s = Co_s \Delta x/(u+c_s)$, for $u \geqslant 0$) of the algorithm becomes very small.

The discussion until now applies to any FVS scheme. We now focus on the schemes described above. We do this by setting $f = F_m^+/F_m$ or $f = F_e^+/F_e$ with F_m and F_e given by Eq. (3), and F_m^+ and F_e^+ from van Leer's polynomials (see Section 3) and by the polynomials of different orders that we have obtained (see Section 4). The resulting values of F_m^+/F_m and F_e^+/F_e as a function of M are shown in Fig. 10.

From this figure, we see that all of the polynomials give $f = 1$ for $M = 1$, and $f \to \infty$ for $M \to 0$. For any given Mach number $0 < M < 1$, the values of f are lower for the polynomials of increasing order.

Therefore, if we take $f = F_m^+/F_m$ or $f = F_e^+/F_e$ (see Fig. 10), the maximum allowed Courant number for stability is $Co_s = 1$ for $M = 1$, and it decreases for $M \to 0$, reaching $Co_s = 0$ for $M = 0$ (as obtained from Eq. (23) for $f \to \infty$, see also Fig. 9).

We should also note that van Leer's forward momentum flux has $F_p^+/F_p = 1$ for $M = 1$, and monotonically decreasing F_p^+/F_p for lower M values, reaching $F_p^+/F_p = 1/2$ at $M = 0$ (see Eqs. (3) and (6)). Therefore, if we set $f = F_p^+/F_p$ we again obtain a vanishingly small maximum allowed Courant number for $M = 1$ (see Eq. (23) and Fig. 9).

The linear stability analysis therefore implies that for $M \to 0$, the maximum allowed timestep $\Delta t_s = Co_s\ \Delta x/(u+c_s)$ (for $u \geqslant 0$) becomes vanishingly small. This property is common to all FVS algorithms with non-zero mass and energy fluxes for $M = 0$. From the many results published in the literature it is clear, however, that in applications of van Leer's FVS scheme to flows with active, low Mach number regions, stable results are obtained by choosing a Courant number of $\sim 0.01 \to 0.1$.

8. Conclusions

We have derived a set of polynomials of order $p \leqslant 10$ for interpolating the mass and energy components of the split fluxes $F^{\pm}$ for the Euler equations in the subsonic, $|M < 1|$ regime. These polynomials are the ones that give the lowest possible value for $|F^{\pm}(M = 0)|$, without having maxima, minima or zeroes in the $|M < 1|$ interval. We derive polynomials of orders 2, 4, 6, 8 and 10 for the forward mass flux, and of orders 4, 6, 8 and 10 for the forward energy flux (the backward flux being given by the relation $F^- = F - F^+$, with F given by Eq. (3)).

Our forward mass and energy fluxes (combined with van Leer's momentum flux, given by Eq. (5)) give Jacobian matrices with two positive and one negative eigenvalue. This in principle violates the basic idea of flux vector splitting algorithms, in which one divides the Euler fluxes into fluxes with strictly positive and strictly negative eigenvalues (transporting linear perturbations in the positive and negative directions, respectively). However, the moduli of the negative eigenvalues are much smaller than the positive eigenvalues. Probably because of this feature, our fluxes give well behaved flow solutions.

We illustrate the behaviour of three combinations of our mass and energy fluxes through an application of a first order implementation of the flux vector splitting algorithm. In particular, we apply the algorithm to one of the Riemann problems used as a test of different algorithms by Toro [7]. We find that all of our fluxes produce somewhat sharper shocks and contact discontinuities than the fluxes of van Leer [4,5]. In particular, if we use our 10th order polynomials for the mass and energy fluxes, we obtain shocks and contact discontinuities that are ~ 20—30% narrower than the ones obtained with van Leer's fluxes.

To summarize, we have calculated interpolations with polynomials on the Mach number of order 2, 4, 6, 8 and 10 for the mass and energy split fluxes. These polynomials are alternatives to the corresponding fluxes of van Leer [4,5], and produce flow solutions with somewhat narrower shocks and contact discontinuities. Even though the improvement obtained over van Leer's algorithm is not very large (~ 20—30% narrower shocks and contact discontinuities), the implementation of the new split fluxes in existing flux vector splitting codes is trivial, and probably worth doing. The behaviour of the different possible combinations of the mass and energy fluxes which we are proposing (see, e.g., Gressier et al. [8]) should be explored in more detail in future work.

References

[1] J.L. Steger, R.F. Warming, Flux-vector splitting of the inviscid gasdynamic equations with application to finite-difference methods, J. Comput. Phys. 40 (1981) 263–293.
[2] M. Sun, K. Takayama, An artificially upstream flux vector splitting scheme for the Euler equations, J. Comput. Phys. 189 (2003) 305–329.
[3] T.K. Sengupta, R. Jain, A. Dipankar, A new flux-vector splitting compact finite volume scheme, J. Comput. Phys. 207 (2005) 261–281.
[4] B. van Leer, Towards the ultimate conservative difference scheme V. – A second-order sequel to Godunov's method, J. Comput. Phys. 32 (1979) 101–136.
[5] B. van Leer, Flux-vector splitting for the Euler equations, ICASE Report No., 1982, pp. 82–30.
[6] W.J. Coirier, B. van Leer, Numerical flux formulas for the Euler and Navier–Stokes equations, NASA TM 104353, AIAA-91-1566, 1991.
[7] E.F. Toro, Riemann Solvers and Numerical Methods for Fluid Dynamics: A Practical Introduction, Springer, Berlin, Heidelberg, 1999.
[8] J. Gressier, P. Villediew, J.-M. Moschetta, Positivity of flux-vector splitting schemes, J. Comput. Phys. 155 (1999) 199–220.
[9] D.R.C. Kelly, P. Korevaar, Type II supernova test cases and breakout modelling with flux-vector splitting and adaptive gridding, Astron. Astrophys. 296 (1995) 418–420.
[10] A.C. Raga, R. Navarro-González, M. Villagrán-Muniz, A new, 3D adaptive grid code for astrophysical and geophysical gasdynamics, Rev. Mex. Astron. Astrof. 36 (2000) 67–76.